ISSN 1996-3343

Asian Journal of Applied Sciences

http://knowledgiascientific.com

Knowledgia SCIENTIFIC
A Place to Publish Outstanding Research

Asian Journal of Applied Sciences 4 (2): 119-136, 2011
ISSN 1996-3343 / DOI: 10.3923/ajaps.2011.119.136
© 2011 Knowledgia Review, Malaysia

Mathematical Modeling of Heat Conduction in a Disk Brake System During Braking

[1]H. Mazidi, [1]S. Jalalifar, [2]S. Jalalifar and [3]J. Chakhoo
[1]Islamic Azad University, Aliabad Katul Branch, Aliabad, Iran
[2]Department of Physics, Neyshabour Branch, Ferdowsi University, Neyshabour, Iran
[3]Department of Physics, Payam Noor University of Gonbad, Gonbad Kavoos, Iran

Corresponding Author: Hoseyn Mazidi, Daneshgah Blvd, Islamic Azad University-Aliabad, Katul Branch, Aliabad, Zip Code 4941793451, Golestan, Iran Tel: +98-911-176-8285 Fax: 0098-21-88806886

ABSTRACT

In this study, the heat conduction problems of the disk brake components (pad and rotor) are modeled mathematically and is solved numerically using Finite Difference Method. In the discretization of time dependant equations the implicit method is taken into account. In the derivation of the heat equations, parameters such as the duration of braking, vehicle velocity, geometries and the dimensions of the brake components, materials of the disk brake rotor and the pad and contact pressure distribution have been taken into account. Results show that there is a heat partition at the contact surface of two sliding components, because of thermal resistance due to the accumulation of wear particles between contact surfaces. This phenomenon prevents absorption of more heat by the discs and causes brake lining to be hot. As a result, heat soaking to the brake fluid increases and may cause brake fluid to evaporate.

Key words: Pad, rotor, finite difference method, heat partition, heat soaking, brake fluid

INTRODUCTION

Brakes are among the most widespread units with nonstationary friction. Braking friction systems are used for damping the kinetic energy of rotational or translational motion of masses by friction forces. By braking, one can decrease the velocity of relative sliding to zero (a stop) or to the given value (a snubbing). In the course of operation of braking units, all parameters of the process (velocity, load, temperature, physicomechanical and friction-wearing characteristics of materials of a couple and conditions of contact) vary. To a great extent, their intensity is determined by the temperature of a frictional contact. In particular, the temperature can be greater than admissible (critical) values for a given material, which leads to undesirable effects, such as local score and grasping. As a result, this can worsen conditions in the contact zone, namely, a decrease in the areas of contour and nominal regions as well as an increase in the temperature and its nonuniformity, which can violate the normal operation of a friction unit (Evtushenko *et al*., 2000).

The friction-induced temperature rise at the interface of two sliding bodies can cause a number of effects, including yield strength reduction, accelerated oxidation wear and thermo-elastic instability, all of which may lead to degradation of performance or even the failure of the associated components. It is of interest, therefore, to accurately determine the temperature field resulting from sliding contact. When one body slides over another body, heat is generated at the interface due to friction and this heat is partitioned between the two bodies. The partitioning of heat is a function

of the thermal properties of the bodies, the contact geometry and the sliding speed (Bansal and Streator, 2008). Shape and physical properties of the brake rotor disc can also affect brake induced problems such as judder (vibration due to rotor warping or uneven disc thickness), fade (loss of brake effectiveness due to frictional heat) and noise. Accordingly, frictional brake pad material should maintain a relatively high, stable and reliable friction coefficient at wide range of braking conditions irrespective of temperature, humidity, age, degree of wear and corrosion, presence of dirt and water spraying from the road, etc. In addition to these, come next safety requirements, long life and high comfort, i.e., absence of vibration and squeal noise (El-Tayeb and Liew, 2009). Thermal stresses due to high temperatures may induce a number of unfavorable conditions such as surface cracks and permanent distortions. Frictional heating, thermal deformation and elastic contact in sliding contact systems affect the contact pressure and temperature on the friction surfaces. If the sliding speed is excessively high, these coupled thermal and mechanical behaviors can be unstable leading to localized high temperature contact regions called hot spots on the sliding interface. The appearance of these hot spots is known as frictionally excited thermoelastic instability or TEI and is observed in many practical applications, especially brakes and clutches (Lee and Jang, 2009; Yi *et al*., 2000; Choi and Lee, 2004; Voldrich, 2006; Li and Barber, 2008; Afferrante and Decuzzi, 2004; Zhu *et al*., 2009; Afferrante *et al*., 2003). Heat generation due to friction in the sliding contact of two bodies influences friction and wear characteristics of brake systems. We note that numerous experimental evidences suggest that the contact area is generally circular, e.g., tread broke railway wheels exhibit circular thermally affected zones on the surface (Yevtushenko and Chapovska, 1997).

In a study by Evtushenko *et al*. (1997) thermo-mechanical processes are studied at the contact area of a metal brake disk and brake block during braking. Expressions are obtained for both the temperature and the thermal displacement in the center of the contact area caused by the effect of the friction heat source, whose power is a linear function of time. Valvano and Lee (2000) proposed a technique to determine the thermal distortion under transient or steady state conditions. Agrawal (2004) presented a Fractional Derivative Approach for thermal analysis of disk brakes. Tribological properties and wear characteristics of automotive disc brakes are presented in many researches (Uyyuru *et al*., 2007; Gudmand-Hoyer *et al*., 1999; Cho *et al*., 2005; Boz and Kurt, 2007; Blau and McLaughlin, 2003; Mosleh *et al*., 2004; Guerin *et al*., 1997). Aerodynamic cooling of high performance disk brake systems is investigated by many researchers (Wallis *et al*., 2002; Johnson *et al*., 2003; McPhee and Johnson, 2007). Gao and Lin (2002) have presented an analytical model for the determination of the contact temperature distribution on the working surface of a brake. To consider the effects of the moving heat source (the pad) with relative sliding speed variation, a transient finite element technique is used to characterize the temperature fields of the solid rotor with appropriate thermal boundary conditions. Numerical results shows that the operating characteristics of the brake exert an essentially influence on the surface temperature distribution and the maximal contact temperature. Dufrenoy (2004) proposed a macro-structural model of the thermo-mechanical behavior of the disk brake, taking into account the real three-dimensional geometry of the disk-pad couple. Contact surface variations, distortions and wear are taken into account. Naji *et al*. (2000) presented a mathematical model to describe the thermal behavior of a brake system which consists of the shoe and the drum. The model is solved analytically using Green's function method for any type of the stopping braking action. The thermal behavior is investigated for three specified braking actions which were the impulse, the unit step and trigonometric stopping actions.

In a study by Talati and Jalalifar (2008), two major models are used for calculation of frictional heat generation: namely macroscopic and microscopic model. In the macroscopic model, the law of conservation of energy or first law of thermodynamics is taken into account. And for the microscopic model, parameters such as the duration of braking, velocity of the vehicle, dimensions and geometry of the brake system, materials of the disk brake rotor and the pad are taken into account. For calculation of prescribed heat flux boundary condition in their model, two kinds of pressure distribution are considered: uniform wear and uniform pressure. In this study, these two models are used. However, in this study the real distribution of contact pressure and velocity changes with respect to time, during braking action is presented. Therefore, more accurate description of how heat generation with respect to time is presented.

MATERIALS AND METHODS

Governing equations in disk brake system: In Fig.1a caliper assembly and Fig. 1b the schematic shape of the disk and the pad in sliding contact is shown. As it is shown disk is like an annulus and pad is like a partial annulus. The brake system clamps the pads through the caliper assembly by brake fluid pressure in the cylinders. Rotary motion of the disk causes a sliding contact between the disk and the pad and generates heat.

For calculation of heat generation due to friction, rate of dissipated heat via friction should be taken into account. This is all to do with the calculation of friction force and rate of work done by friction force. For calculation of friction force, the pressure distribution at the contact surface of the disk and the pad should be determined. Here, two types of pressure distribution are taken into accounts:

Uniform pressure distribution: When the pad is new and short enough the pressure is distributed uniformly in the contact area that is:

$$p = p_{max} \tag{1}$$

Uniform wear: After several braking action when the pad is rundown this type of pressure distribution is taken into account because work done by friction force grows when the radial

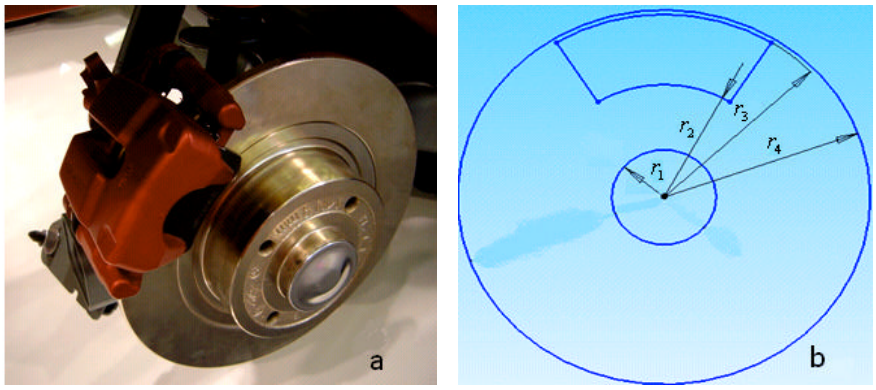

Fig. 1: (a) Disk brake system and caliper assembly and (b) schematic shape of the disk and the pad in sliding contact

distance increases and eventually the farther radial position is more encountered to wear and the assumption of uniform pressure distribution is no longer dominant. In this situation pressure distribution in the pad is proportional to 1/r and maximum pressure occurs at $r = r_2$.

$$\delta = kpr = const \Rightarrow p = p_{max}\frac{r_2}{r} \quad (2)$$

where, δ is wear, p_{max} is the maximum pressure distributed in the pad and p is the pressure at radial position r.

Heat generation due to friction: In the contact area of brake components; the pads and the disk; heat is generated due to friction. For calculation of heat generation at the interface of these two sliding bodies' two methods is suggested:

- At the basis of law of conservation of energy the kinetic energy of the vehicle during motion is equal to the dissipated heat after vehicle stop
- By knowing the friction coefficient, pressure distribution at the contact area, geometric characteristics of the pad and the disk, relative sliding velocity and duration of braking action one can calculate the heat generated due to friction

Here, these two types are illustrated:

Macroscopic model: Brakes are essentially a mechanism to change the energy types. When a car is moving with speed, it has kinetic energy. Applying the brakes, the pads or shoes that press against the brake drum or rotor convert this energy into thermal energy. The cooling of the brakes dissipates the heat and the vehicle slows down. This is all to do with the first law of thermodynamics, sometimes known as the law of conservation of energy that states that energy cannot be created nor destroyed; it can only be converted from one form to another. In the case of brakes, it is converted from kinetic energy to thermal energy:

$$E_c = \frac{1}{2}MV_0^2 \quad (3)$$

where, M is the total mass of the vehicle and V_0 is the initial speed of the vehicle. To obtain the amount of heat dissipated by each of the front brake disks, we should know the weight distribution of the vehicle. So, the amount of heat dissipated by each of the disks will be:

$$Q = 0.5 \times \frac{1}{2}mV_0^2 = 0.25mV_0^2 \quad (4)$$

where, m is the amount of the distributed mass on the front axle of the vehicle.

Microscopic model: Rate of generated heat due to friction is equal to the friction power. Some of this frictional heat is absorbed by the disk and the rest is absorbed by the pads. If it is supposed that the whole friction power is transferred to heat energy and heat partition coefficient is stated by the parameter σ then we have the following relations for heat generation.

Heat generation: Contact surface element of the disk and the pad is shown in Fig. 2a and b, respectively. The rate of heat generated due to friction between these surfaces is calculated as follows:

$$d\dot{E} = dP = VdF_f = r\omega\mu p\phi_0 rdr \tag{5a}$$

$$d\dot{E} = d\dot{E}_p + d\dot{E}_d \tag{5b}$$

$$d\dot{E}_p = (1-\sigma)dP = (1-\sigma)\mu p\omega\phi_0 r^2 dr \tag{5c}$$

$$d\dot{E}_d = \sigma dP = \sigma\mu p\phi_0\omega r^2 dr \tag{5d}$$

where, $d\dot{E}$ is the rate of heat generated due to friction between two sliding components, V is the relative sliding velocity and dF_f is the friction force. The terms $d\dot{E}_p$ and $d\dot{E}_d$ are the amount of absorbed heat by the pad and the disk, respectively. The parameter σ is defined as:

$$\sigma = \frac{\xi_d S_d}{\xi_d S_d + \xi_p S_p} \tag{6}$$

where, ξ_p and ξ_d are the thermal effusivities of the pad and the disk and S_p and S_d are frictional contact surfaces of the pad and the disk, respectively. Thermal effusivity is defined as:

$$\xi = \sqrt{k\rho c} \tag{7}$$

Heat flux: To obtain the heat flux at the surfaces of two components of the brake system, we divide rate of thermal energy by the surface contact area of each component.

- Heat flux in the pad

$$q_1(r,t) = \frac{d\dot{E}_p}{dS_p} = (1-\sigma)\mu p(t) r\omega(t) \tag{8}$$

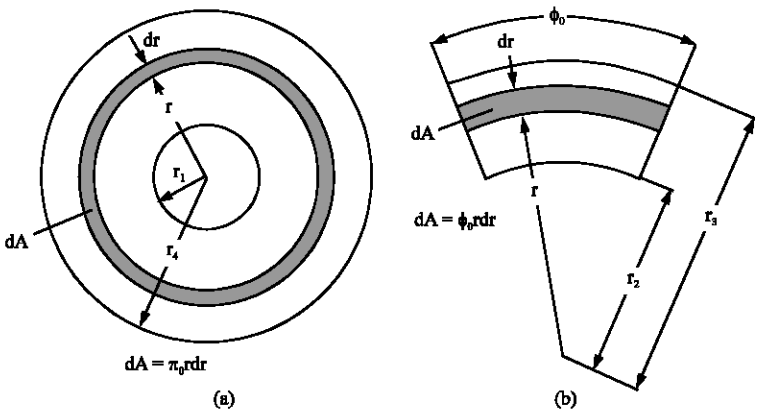

Fig. 2: Contact surface element of two components (a) the disk and (b) the pad

- Heat flux in the disk

$$q_2(r,t) = \frac{d\dot{E}_d}{dS_d} = \frac{\phi_0}{2\pi}\lambda\mu p(t) r\omega(t) \tag{9}$$

Heat flux for uniform pressure is a function of time and space variable r; the angular velocity decreases with time during braking action and the work done by friction force grows as radial space variable increases. Heat flux obtained for the uniform wear is just a function of time and it is independent of the space variable; the work done by friction force is the same at radial direction.

Heat equation for the pad: Figure 3 shows the two dimensional thermal problem of the pad for two assumption of pressure distribution; uniform wear and uniform pressure in Fig. 3a and b, respectively. Heat equation and the appropriate boundary conditions for the pad may be written in the following form:

$$\frac{\partial^2 T}{\partial r^2} + \frac{1}{r}\frac{\partial T}{\partial r} + \frac{\partial^2 T}{\partial z^2} = \frac{1}{\alpha}\frac{\partial T}{\partial t} \;\; ; \;\; r_2 < r < r_3 \;\; , \;\; 0 < z < d_1 \;\; , \;\; t > 0 \tag{10a}$$

$$-\frac{\partial T}{\partial r} + HT = HT_\infty \;\; ; \;\; r = r_2 \;\; ; \;\; 0 \le z \le d_1 \;\; , \;\; t \ge 0 \tag{10b}$$

$$\frac{\partial T}{\partial r} + HT = HT_\infty \;\; ; \;\; r = r_3 \;\; ; \;\; 0 \le z \le d_1 \;\; , \;\; t \ge 0 \tag{10c}$$

$$\frac{\partial T}{\partial z} = q_1(r,t) \;\; ; \;\; z = 0 \;\; ; \;\; r_2 \le r \le r_3 \;\; , \;\; t \ge 0 \tag{10d}$$

$$\frac{\partial T}{\partial z} = 0 \;\; ; \;\; z = d_1 \;\; ; \;\; r_2 \le r \le r_3 \;\; , \;\; t \ge 0 \tag{10e}$$

$$T(r,z,0) = T_0 \;\; ; \;\; r_2 \le r \le r_3 \;\; , \;\; 0 \le z \le d_1 \tag{10f}$$

Discretization of heat conduction problem of the pad: Figure 4 shows meshing of the finite difference method of the pad. For discretization of the equations the variables r, z and t are defined as:

$$r = i\Delta r; \; i = 0,1,2,\ldots,48 \tag{10g}$$

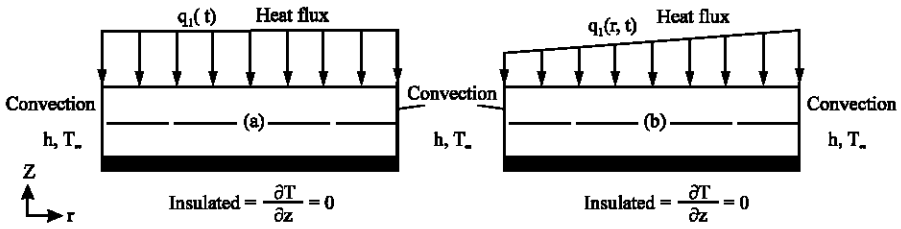

Fig. 3: Boundary conditions for the pad (a) uniform wear and (b) uniform pressure

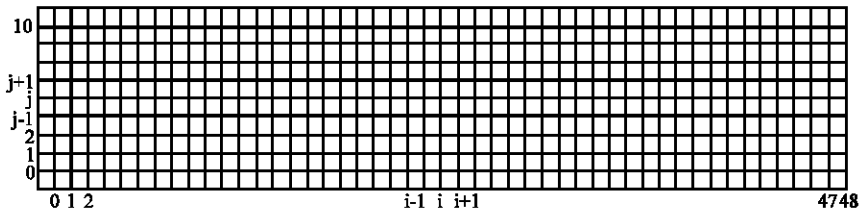

Fig. 4: Finite difference discretization of the pad

$$z = j\Delta z;\ j = 0,1,2,...,10 \tag{10h}$$

$$t = n\Delta t;\ n = 0,1,2,... \tag{10i}$$

Here, the difference in the radial and axial direction is taken the same that is $\Delta r = \Delta z = L = 0.001$ m. For obtaining the temperatures of various nodes, the heat equations of interior nodes and boundary nodes must be considered separately.

Interior nodes: For interior nodes (i = 1, 2,..,47; j = 1, 2,...,9) of the pad shown in Fig. 4 the finite difference model of heat conduction can be written in the following form:

$$T_{i,j}^{(n+1)} = \frac{1}{(1+4s_1)}\left[T_{i,j}^{(n)} + s_1 T_{i,j+1}^{(n+1)} + s_1 T_{i,j-1}^{(n+1)} + (s_1 - \frac{s_2}{r_1 + iL})T_{i-1,j}^{(n+1)} + (s_1 + \frac{s_2}{r_1 + iL})T_{i+1,j}^{(n+1)}\right] \tag{11}$$

where, s_1 and s_2 are defined as: $s_1 = \frac{\alpha\Delta t}{L^2}$ and $s_2 = \frac{\alpha\Delta t}{2L}$.

Boundary nodes

The boundary at r = r_2: As it can be seen from Fig. 5 at this boundary i = 0 is constant and j varies from 1 to 9 (except for nodes at the corner j = 0 and j = 10). The nodes -1, j is obtained from virtual expansion of boundary nodes. So, finite difference equations of these nodes can be stated as:

$$T_{0,j}^{(n+1)} = \frac{1}{(1+4s_1)}\left[T_{0,j}^{(n)} + s_1 T_{0,j+1}^{(n+1)} + s_1 T_{0,j-1}^{(n+1)} + 2LH(s_1 - \frac{s_2}{r_2})(T_\infty - T_{0,j}^{(n+1)}) + 2s_1 T_{1,j}^{(n+1)}\right] \tag{12}$$

The boundary at r = r_3: Meshing of this boundary is like Fig. 5 but at this boundary i = 48 is constant and j varies from 1 to 9 (except for nodes at the corner j = 0 and j = 10). The nodes -47 is obtained from virtual expansion of boundary nodes. So, finite difference equations of these nodes can be stated as:

$$T_{48,j}^{(n+1)} = \frac{1}{(1+4s_1)}\left[T_{48,j}^{(n)} + s_1 T_{48,j+1}^{(n+1)} + s_1 T_{48,j-1}^{(n+1)} + 2s_1 T_{47,j}^{(n+1)} + 2LH(s_1 + \frac{s_2}{r_3})(T_\infty - T_{48,j}^{(n+1)})\right] \tag{13}$$

The boundary at z = 0: As it is shown in Fig. 6, at this boundary j = 0 is constant and index i varies from 1 to 47 (except for nodes at the corner i = 0 and i = 48). The nodes i, -1 are obtained from virtual expansion of boundary nodes finite difference equations of these nodes can be stated as:

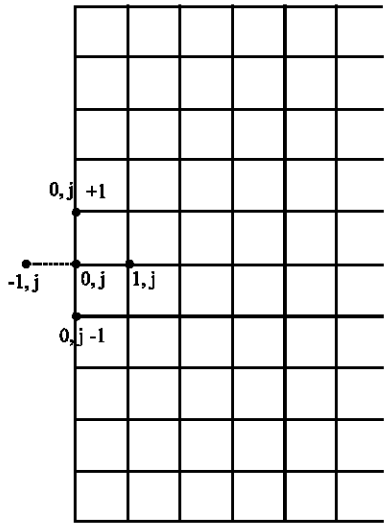

Fig. 5: Meshing at $r = r_2$

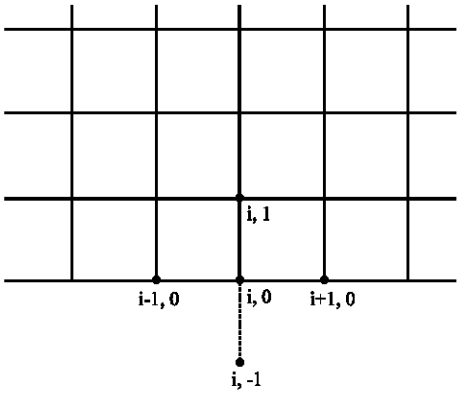

Fig. 6: Meshing at z = 0

$$T_{i,0}^{(n+1)} = \frac{1}{(1+4s_1)}\left[T_{i,0}^{(n)} + 2s_1 T_{i,1}^{(n+1)} - 2Ls_1 q_l(r_2 + iL, n\Delta t) + (s_1 - \frac{s_2}{r_2 + iL})T_{i-1,0}^{(n+1)} + (s_1 + \frac{s_2}{r_2 + iL})T_{i+1,0}^{(n+1)}\right] \quad (14)$$

The boundary at $z = d_1$: Meshing of this boundary is similar to Fig. 6 but at this boundary j = 10 is constant and index i varies from 1 to 47 (except for nodes at the corner i = 0 and i = 48). Finite difference equations of these nodes can be stated as:

$$T_{i,10}^{(n+1)} = \frac{1}{(1+4s_1)}\left[T_{i,10}^{(n)} + 2s_1 T_{i,9}^{(n+1)} + (s_1 - \frac{s_2}{r_1 + iL})T_{i-1,10}^{(n+1)} + (s_1 + \frac{s_2}{r_1 + iL})T_{i+1,10}^{(n+1)}\right] \quad (15)$$

Nodes that are in the corner

Intersection of two boundary conditions at $r = r_2$ and z = 0: As it is shown in Fig. 7 at this point both indices of i and j are equal to zero. The nodes -1, 0 and 0, -1 is obtained from virtual expansion of boundary nodes. Finite difference equation of this single node can be stated as:

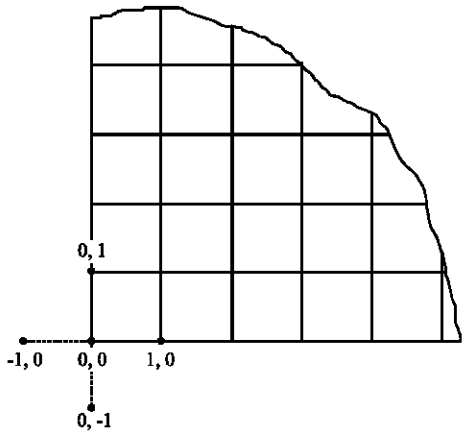

Fig. 7: Meshing at the intersection of two boundary conditions of $r = r_2$ and $z = 0$

$$T_{0,0}^{(n+1)} = \frac{1}{(1+4s_1)}\left[T_{0,0}^{(n)} + 2s_1T_{0,1}^{(n+1)} - 2Ls_1q_1(r_2, n\Delta t) + 2LH(s_1 - \frac{s_2}{r_2})(T_\infty - T_{-1,0}^{(n+1)}) + 2s_1T_{1,0}^{(n+1)}\right] \quad (16)$$

Intersection of two boundary conditions at $r = r_3$ and $z = 0$: At this point the index i = 48 and j is equal to zero. The nodes -47, 0 and 48, -1 is obtained from virtual expansion of boundary nodes. Finite difference equation of this single node can be stated as:

$$T_{48,0}^{(n+1)} = \frac{1}{(1+4s_1)}\left[T_{48,0}^{(n)} + 2s_1T_{48,1}^{(n+1)} - 2Ls_1q_1(r_3, n\Delta t) + (s_1 - \frac{s_2}{r_3})T_{47,0}^{(n+1)} + 2LH(s_1 + \frac{s_2}{r_3})(T_\infty - T_{48,0}^{(n+1)})\right] \quad (17)$$

Intersection of two boundary conditions at $r = r_2$ and $z = d_1$: At this point the index i = 0 and j = 10. The nodes -1, 10 and 0, -9 is obtained from virtual expansion of boundary nodes. Finite difference equation of this single node can be stated as:

$$T_{0,10}^{(n+1)} = \frac{1}{(1+4s_1)}\left[T_{0,10}^{(n)} + 2s_1T_{0,9}^{(n+1)} + 2LH(s_1 - \frac{s_2}{r_2})(T_\infty - T_{0,10}^{(n+1)}) + 2s_1T_{1,10}^{(n+1)}\right] \quad (18)$$

Intersection of two boundary conditions of $r = r_3$ and $z = d_1$: At this point the index i = 48 and j = 10. The nodes -47, 10 and 48, -9 is obtained from virtual expansion of boundary nodes. Finite difference equation of this single node can be stated as:

$$T_{48,10}^{(n+1)} = \frac{1}{(1+4s_1)}\left[T_{48,10}^{(n)} + 2s_1T_{48,9}^{(n+1)} + 2s_1T_{47,10}^{(n+1)} + 2LH(s_1 + \frac{s_2}{r_3})(T_\infty - T_{48,10}^{(n+1)})\right] \quad (19)$$

Heat equation for the disk: Figure 8 shows the boundary conditions of the disk for two types of pressure distribution; uniform pressure and uniform wear in Fig. 8a and b, respectively. As it can be seen, since the thermal problem in the disk is symmetric in z direction, only the half of the

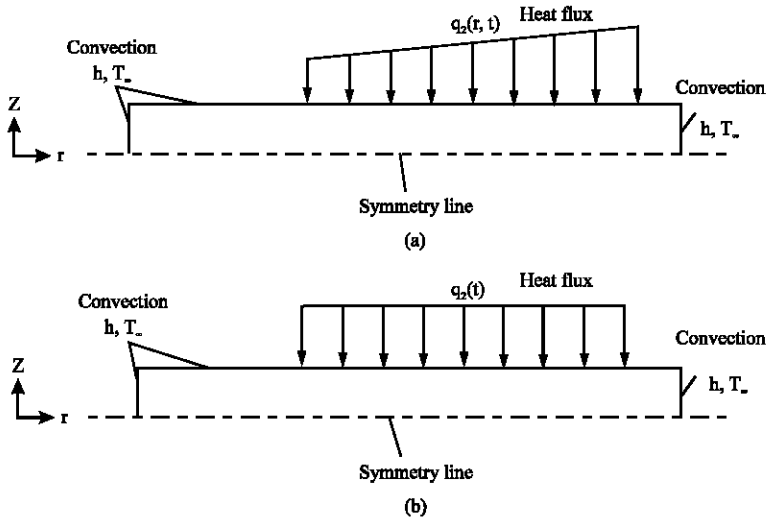

Fig. 8: Boundary conditions for the disk (a) uniform pressure and (b) uniform wear

disk $(z_2 = \frac{d_2}{2})$ is considered. So, the transient heat equation for the disk and related boundary conditions that have been shown on Fig. 8 may be formulated as:

$$\frac{\partial^2 T}{\partial r^2} + \frac{1}{r}\frac{\partial T}{\partial r} + \frac{\partial^2 T}{\partial z^2} = \frac{1}{\alpha}\frac{\partial T}{\partial t} \; ; \; r_1 < r < r_4 \; , \; 0 < z < z_2 \; , \; t > 0 \tag{20a}$$

$$-\frac{\partial T}{\partial r} + HT = HT_\infty \; ; \; r = r_1 \; , \; 0 \le z \le z_2 \; , \; t \ge 0 \tag{20b}$$

$$\frac{\partial T}{\partial r} + HT = HT_\infty \; ; \; r = r_4 \; , \; 0 \le z \le z_2 \; , \; t \ge 0 \tag{20c}$$

$$\frac{\partial T}{\partial z} = 0 \; ; \; z = 0 \; , \; r_1 \le r \le r_4, \; t \ge 0 \tag{20d}$$

$$\frac{\partial T}{\partial z} + HT = HT_\infty \; ; \; z = z_2 \; , \; r_1 \le r \le r_2, \; r_3 \le r \le r_4 \; , \; t \ge 0 \tag{20e}$$

$$\frac{\partial T}{\partial z} = q_2(r,t) \; ; \; z = z_2 \; , \; r_2 \le r \le r_3 \; , \; t \ge 0 \tag{20f}$$

$$T(r,z,0) = T_0 \; ; \; r_1 \le r \le r_3 \; , \; 0 \le z \le d_2 \tag{20g}$$

Discretization of heat conduction problem of the disk: Discretization of heat conduction of the disk is quite similar to the pad. However the space differences in the radial and axial direction are taken as $\Delta r = \Delta z = L = 0.00025$ m. For obtaining the temperatures of various nodes as before, the heat equations of interior nodes and boundary nodes must be considered separately.

Interior nodes: For interior nodes (i = 1, 2,...381; j = 1, 2,...,24) of the disk, the finite difference model of heat conduction can be written in the following form:

$$T_{i,j}^{(n+1)} = \frac{1}{(1+4s_1)}\left[T_{i,j}^{(n)} + s_1 T_{i,j+1}^{(n+1)} + s_1 T_{i,j-1}^{(n+1)} + (s_1 - \frac{s_2}{r_1 + iL})T_{i-1,j}^{(n+1)} + (s_1 + \frac{s_2}{r_1 + iL})T_{i+1,j}^{(n+1)}\right] \quad (21)$$

where, s_1 and s_2 are defined before.

Boundary nodes

Boundary conditions at r = r_1: This boundary condition is similar to the boundary condition of the pad at r = r_2. At this boundary i = 0 is constant and j = 1, 2,...24.

$$T_{0,j}^{(n+1)} = \frac{1}{(1+4s_1)}\left[T_{0,j}^{(n)} + s_1 T_{0,j+1}^{(n+1)} + s_1 T_{0,j-1}^{(n+1)} + 2LH(s_1 - \frac{s_2}{r_1})(T_\infty - T_{0,j}^{(n+1)}) + 2s_1 T_{1,j}^{(n+1)}\right] \quad (22)$$

Boundary conditions at r = r_4: This boundary condition is similar to the boundary condition of the pad at r = r_3. At this boundary i = 382 is constant and j = 1, 2,...,24.

$$T_{382,j}^{(n+1)} = \frac{1}{(1+4s_1)}\left[T_{382,j}^{(n)} + s_1 T_{382,j+1}^{(n+1)} + s_1 T_{382,j-1}^{(n+1)} + 2s_1 T_{381,j}^{(n+1)} + 2LH(s_1 + \frac{s_2}{r_4})(T_\infty - T_{382,j}^{(n+1)})\right] \quad (23)$$

Boundary condition at z = 0: This boundary condition is similar to the boundary condition of pad at z = 0. At this boundary j = 0 is constant and i = 1, 2,...,381.

$$T_{i,0}^{(n+1)} = \frac{1}{(1+4s_1)}\left[T_{i,0}^{(n)} + 2s_1 T_{i,1}^{(n+1)} + (s_1 - \frac{s_2}{r_1 + iL})T_{i-1,0}^{(n+1)} + (s_1 + \frac{s_2}{r_1 + iL})T_{i+1,0}^{(n+1)}\right] \quad (24)$$

Boundary condition at z = z_2: At this boundary j = 25 is constant but as it can be seen in Fig. 8 this boundary should be considered in three sections. Two of them are exposed to the boundary condition of the third kind or convection (i = 1, 2,...,177 and i = 370, 371,...,381) and the other is exposed to the boundary condition of the second kind or prescribed heat flux (i = 178, 179,...,369). So, the boundary condition in this three section can be formulated as:

Boundary nodes at z = z_2 in sections $r_1 \le r \le r_2$ and $r_3 \le r \le r_4$:

$$T_{i,25}^{(n+1)} = \frac{1}{(1+4s_1)}\left[T_{i,25}^{(n)} + 2s_1 LH(T_\infty - T_{i,25}^{(n+1)}) + 2s_1 T_{i,25}^{(n+1)} + (s_1 - \frac{s_2}{r_1 + iL})T_{i-1,25}^{(n+1)} + (s_1 + \frac{s_2}{r_1 + iL})T_{i+1,25}^{(n+1)}\right] \quad (25)$$

Boundary nodes at z = z_2 in section $r_2 \le r \le r_3$:

$$T_{i,25}^{(n+1)} = \frac{1}{(1+4s_1)}\left[T_{i,25}^{(n)} + 2Ls_1 q_2(r_1 + iL, \Delta t) + 2s_1 T_{i,24}^{(n+1)} + (s_1 - \frac{s_2}{r_1 + iL})T_{i-1,25}^{(n+1)} + (s_1 + \frac{s_2}{r_1 + iL})T_{i+1,25}^{(n+1)}\right] \quad (26)$$

Nodes that are in the corner

Intersection of two boundary conditions at $r = r_1$ and $z = 0$: This boundary is similar to the boundary of $r = r_2$ and $z = 0$ for the pad. In this point both i and j is equal to zero. Temperature of this node can be stated as:

$$T_{0,0}^{(n+1)} = \frac{1}{(1+4s_1)}\left[T_{0,0}^{(n)} + 2s_1T_{0,1}^{(n+1)} + 2LH(s_1 - \frac{s_2}{r_1})(T_\infty - T_{0,0}^{(n+1)}) + 2s_1T_{1,0}^{(n+1)}\right] \quad (27)$$

Intersection of two boundary conditions at $r = r_4$ and $z = 0$: This boundary is similar to the boundary of $r = r_3$ and $z = 0$ for the pad. In this point $j = 0$ and $i = 382$. Temperature of this node can be stated as:

$$T_{382,0}^{(n+1)} = \frac{1}{(1+4s_1)}\left[T_{382,0}^{(n)} + 2s_1T_{382,1}^{(n+1)} + 2s_1T_{381,0}^{(n+1)} + 2LH(s_1 + \frac{s_2}{r_4})(T_\infty - T_{382,0}^{(n+1)})\right] \quad (28)$$

Intersection of two boundary conditions at $r = r_1$ and $z = z_2$: At this boundary $i = 0$ and $j = 25$. Temperature of this node can be stated as:

$$T_{0,25}^{(n+1)} = \frac{1}{(1+4s_1)}\left[T_{0,25}^{(n)} + 2s_1T_{0,24}^{(n+1)} + 2LH(2s_1 - \frac{s_2}{r_1})(T_\infty - T_{0,25}^{(n+1)}) + 2s_1T_{1,25}^{(n+1)}\right] \quad (29)$$

Intersection of two boundary conditions at $r = r_4$ and $z = z_2$:

$$T_{382,25}^{(n+1)} = \frac{1}{(1+4s_1)}\left[T_{382,25}^{(n)} + 2s_1T_{382,24}^{(n+1)} + 2s_1T_{381,25}^{(n+1)} + 2LH(2s_1 + \frac{s_2}{r_4})(T_\infty - T_{382,25}^{(n+1)})\right] \quad (30)$$

Brake system data: In Table 1, the dimensions and operating conditions of the disk and the pad is presented. Disk material is steel and pad is composed of an organic composite material.

Table 1: Vehicle brake data (Gao and Lin, 2002)

Items	Disk	Pad
Inner radius (mm)	32.5	77
Outer radius (mm)	128	125
Thickness (mm)	12.5	10
Specific heat (J/kg/K)	419	1465
Thermal conductivity (W/m/k)	48.46	12.12
Density (kg m^{-3})	7228	2595
Pad contact angle (degree)	64.5	
Front axle load (kg)	837	
Tire radius (mm)	314	
Atmospheric temperature T_0 (°C)	20	
The nominal brake pressure value that the skid cannot occur P_0 (MPa)	3.17	
Initial vehicle speed V (m sec^{-1})	27.78	

RESULTS AND DISCUSSION

Figure 9 shows the maximum contact surface temperatures of pad and disc with the assumptions of uniform pressure distribution and uniform wear. As it can be seen, the resulting temperature distribution for uniform pressure is more than the uniform wear mode. Because in the uniform pressure case, the work done by friction force grows as radial distance increases. Whereas the work done in the case of uniform wear does not change in radial distance. As it is clear from the figure, there is a temperature difference between surfaces of the disk and the pad. This is because the thermal resistance between the pad and the disc due to the accumulation of wear particles and the layer object called third body. Therefore, this resistance creates heat partition between the pad and the disc.

As it is clear from Fig. 10, disk surface temperature in the radial interval 35-77 mm, where the disc is exposed to air flow is relatively low. But in the interval 77-125 mm, where the disc is in contact with friction linings, the temperature will increase because in the case of uniform pressure distribution, heat generation grows in the radial distance. However, because the disk is exposed convection air flow in the interval 125-128 mm, in this area temperature will drop.

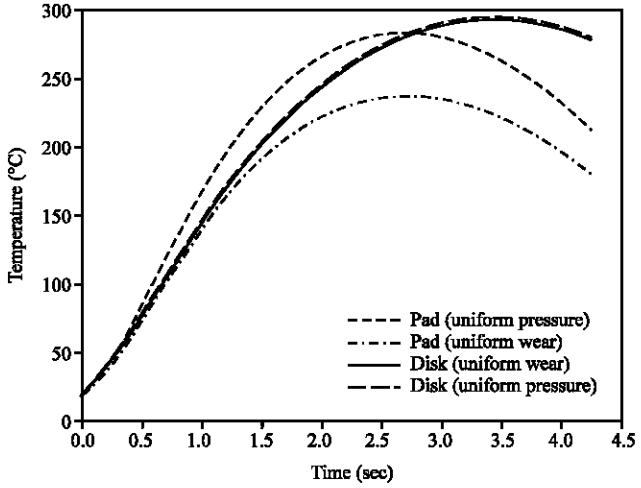

Fig. 9: Maximum contact surface temperature of the disk and the pad with respect to time

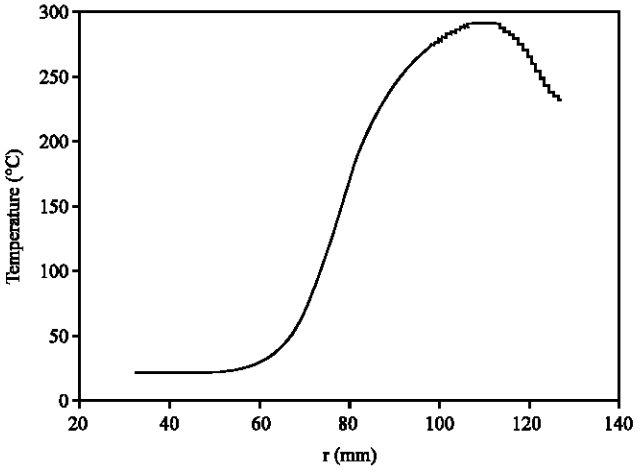

Fig. 10: Disk surface temperature versus radius (uniform pressure)

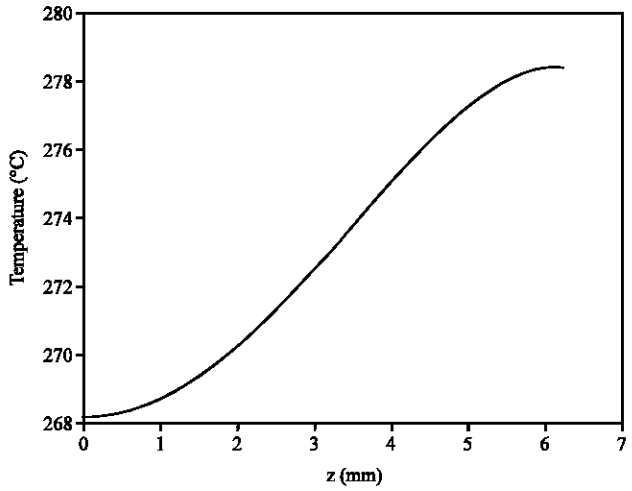

Fig. 11: Disk temperature versus axial position z (uniform pressure)

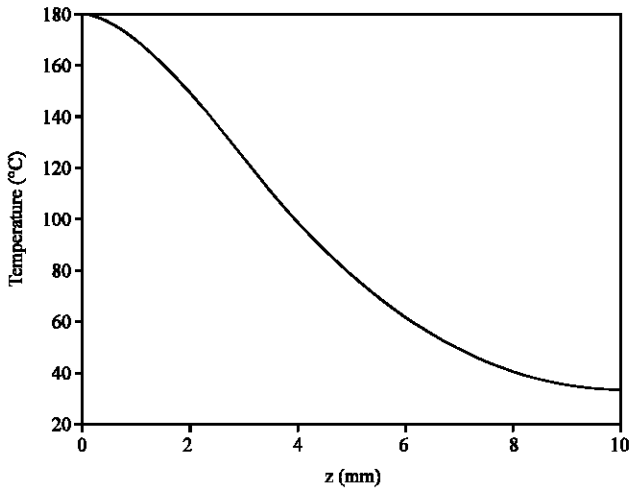

Fig. 12: Pad temperature at position of mean effective radius with respect to z-axis (uniform pressure)

In Fig. 11 temperature distribution with respect to disk thickness at the end of braking action has been shown.

In Fig. 12, pad contact surface temperature at the end of braking action has been shown. As it can be seen, pad contact surface temperature is relatively high. But the other end of the pad temperature that is in contact with caliper assembly well controlled by a layer of insulation. So, the brake fluid vaporization is reduced.

In Fig.13, disk surface temperature changes in different radial locations are shown with respect to time. As it is seen radial disk surface temperature is constant at radial position r = 52 mm which shows that the convection boundary condition in this area is appropriate.

Form Fig. 14 it can be seen that at the start of braking action, disc surface temperature is more than any other axial positions. All graphs plotted merge at the end of braking action which represents that the higher portion of heat generation due to friction (approximately 90.88%) at

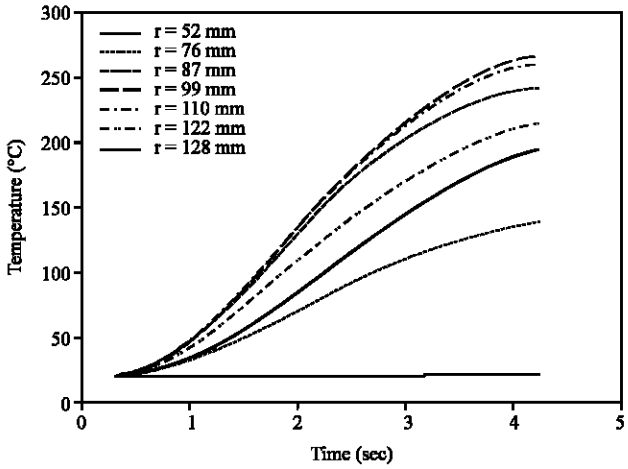

Fig. 13: Disk temperature distribution in radial distances with respect to time (uniform wear)

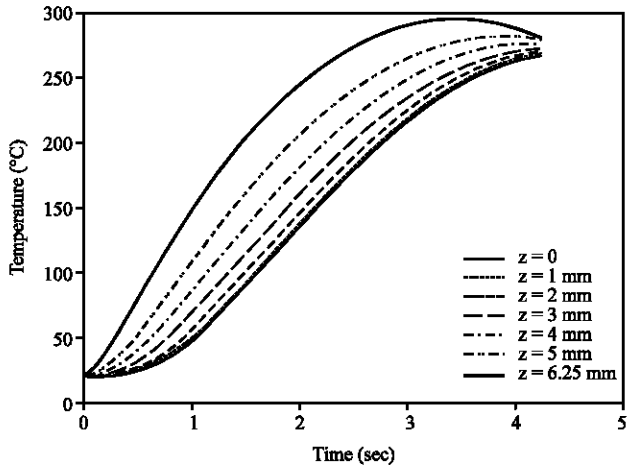

Fig. 14: Disk temperature in different axial positions with respect to time (uniform wear)

the disc and pad contact surface is absorbed by the disk. This high amount of absorbed heat must be dissipated to the environment through the disc via convection.

As it can be seen in Fig. 15, pad temperature at the disk-pad interface (z = 0) has the highest value and gradually decreases when z increases to reach the location z = 10 mm. On the other hand, the slope of temperature graph with respect to time, i.e., $\left.\frac{\partial T}{\partial t}\right|_{t=0}$, in place z = 0 has the maximum value. So, at this location temperature changes rapidly with time. Behavior like this for the other curves at locations z =1, 2 mm can be seen. But in place of z = 6, 10 mm this phenomenon doesn't occur and the slope of the graph decreases until the position z reaches z =10 mm. In this location the slope of temperature - time graph is increased with time means that with time the temperature is increased. If for any reason this braking action is repeated (e.g., repeated braking during high mountain decent), this phenomenon especially for disc brakes equipped with aluminum caliper may be a concern because it may cause brake fluid vaporization. On the other hand, maximum increasing temperature of the brake fluid is often happens during the heat soaking or when the car is parked after several repeated braking.

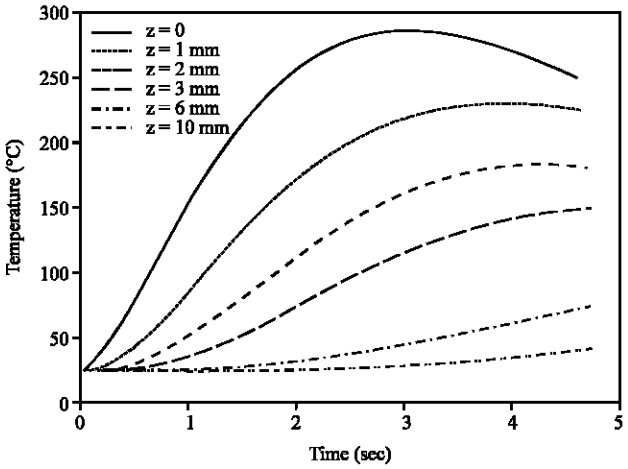

Fig. 15: Pad temperature with respect to time at different axial positions (uniform wear)

CONCLUSIONS

Results for contact surface temperature of the pad and the disc show that there is a heat partition at the contact surface of two sliding components. This is because of thermal resistance due to the accumulation of wear particles between contact surfaces of the pad and the disc and lack of necessary provisions to convection heat loss through the disk to the surrounding.

Contact thermal resistance at the surfaces of the pad and the disk prevent absorption of more heat by the discs and causes brake lining to be hot. As a result, heat soaking to the brake fluid increases and may cause brake fluid to evaporate. So, the brake fluid regarding to minimum wet and dry boiling point with appropriate DOT ratings should be used.

As you know, caliper assembly is located at the end of the pad. If the pad becomes too hot, it may increase the temperature of the brake fluid and causes evaporation. Therefore, it is recommended that the material with low thermal conductivity for the pad and caliper components is used.

If the thickness of the pad is reduced due to excessive wear, influence of heat into the pad and caliper assembly increases and the risk of brake fluid vaporization will increase.

REFERENCES

Afferrante, L., M. Ciavarella, P. Decuzzi and G. Demelio, 2003. Transient analysis of frictionally excited thermoelastic instability in multi-disk clutches and brakes. Wear, 254: 136-146.

Afferrante, L. and P. Decuzzi, 2004. The effect of engagement laws on the thermomechanical damage of multidisk clutches and brakes. J. Wear, 257: 66-72.

Agrawal, O.P., 2004. Application of fractional derivatives in thermal analysis of disk brakes. Nonlinear Dynamics, 38: 191-206.

Bansal, D.G. and J.L. Streator, 2008. A method for obtaining the temperature distribution at the interface of sliding bodies. Wear, 266: 721-732.

Blau, P.J. and J.C. McLaughlin, 2003. Effects of water films and sliding speed on the frictional behavior of truck disc brake material. Trib. Int., 36: 709-715.

Boz, M. and A. Kurt, 2007. The effect of Al2O3 on the friction performance of automotive brake friction materials. J. Tribo. Int., 40: 1161-1169.

Cho, M.H., K.H. Cho, S.J. Kim, D.H. Kim and H. Jang, 2005. The role of transfer layers on friction characteristics in the sliding interface between friction materials against gray iron brake disks. Trib. Lett., 20: 101-108.

Choi, J. and I. Lee, 2004. Finite element analysis of transient thermoelastic behaviors in disk brakes. Wear, 257: 47-58.

Dufrenoy, P., 2004. Two-/three-dimensional hybrid model of the thermomechanical behavior of disc brakes. J. Rail Rapid Transit., 218, Part F: 17-30.

El-Tayeb, N.S.M. and K.W. Liew, 2009. On the dry and wet sliding performance of potentially new frictional brake pad materials for automotive industry. Wear, 266: 275-287.

Evtushenko, A.A., N.V. Gorbacheva and E.G. Ivanik, 1997. Thermomechanical processes in the friction heating of disk brakes. J. Eng. Phys. Thermophys., 70: 113-118.

Evtushenko, O.O., E.H. Ivanyk and N.V. Horbachova, 2000. Analytic methods for thermal calculation of brakes (review). Materials Sci., 36: 857-862.

Gao, C.H. and X.Z. Lin, 2002. Transient temperature field analysis of a brake in a non-axisymmetric three-dimensional model. J. Mat. Proc. Technol., 129: 513-517.

Gudmand-Hoyer, L., A. Bach, G.T. Nielsen and P. Morgen, 1999. Tribological properties of automotive disc brakes with solid lubricants. J. Wear., 232: 168-175.

Guerin, J.D., J.P. Bricout, K. Laden and M. Watremez, 1997. High thermal diffusivity materials for railway brake discs. Tribol. Lett., 3: 257-267.

Johnson, D.A., B.A. Sperandei and R. Gilbert, 2003. Analysis of the flow through a vented automotive brake rotor. J. Fluids. Eng., 125: 979-986.

Lee, S.W. and Y.H. Jang, 2009. Effect of functionally graded material on frictionally excited thermoelastic instability. Wear, 266: 139-146.

Li, J. and J.R. Barber, 2008. Solution of transient thermoelastic contact problems by the fast speed expansion method. Wear, 265: 402-410.

McPhee, A.D. and D.A. Johnson, 2007. Experimental heat transfer and flow analysis of a vented brake rotor. Int. J. Thermal., Sci., 47: 458-467.

Mosleh, M., P.J. Blau and D. Dumitrescu, 2004. Characteristics and morphology of wear particles from laboratory testing of disk brake materials. J. Wear, 256: 1128-1134.

Naji, M., M. Al-Nimr and S. Masoud, 2000. Transient thermal behavior of a cylindrical brake system. J. Heat Mass Transfer, 36: 45-49.

Talati, F. and S. Jalalifar, 2008. Investigation of heat transfer phenomena in a ventilated disk brake rotor with straight radial rounded vanes. J. Applied Sci., 8: 3583-3592.

Uyyuru, R.K., M.K. Surappa and S. Brusethaug, 2007. Tribological behavior of Al-Si-SiCp composites/automobile brake pad system under dry sliding conditions. J. Tribo. Int., 40: 365-373.

Valvano, T. and K. Lee, 2000. An analytical method to predict thermal distortion of a brake rotor. SAE, World Congress, Detroit, Michigan. March 6-9. American Technical Publishers Ltd., USA., pp: 566-571.

Voldrich, J., 2006. Frictionally excited thermoelastic instability in disc brakes-transient problem in the full contact regime. Int. J. Mech. Sci., 49: 129-137.

Wallis, L., E. Leonardi, B. Milton and P. Joseph, 2002. Air flow and heat transfer in ventilated disk brake rotors with diamond and tear-drop pillars. Numerical Heat Transfer Part A, 41: 643-655.

Yevtushenko, A. and R. Chapovska, 1997. Effect of time-dependent speed on frictional heat generation and wear in transient axisymmetrical contact of sliding. Arc. Appl. Mech., 67: 331-338.

Yi, Y., J.R. Barber and P. Zagrodzki, 2000. Eigenvalue solution of thermoelastic instability problems using Fourier reduction. Proc. R. Soc., 456: 2799-2821.

Zhu, Z., Y. Peng, Z. Shi and G. Chen, 2009. Three-dimensional transient temperature field of brake shoe during hoist's emergency braking. Applied Thermal Eng., 29: 932-937.